

# Lawrence Berkeley National Laboratory

## Recent Work

### Title

Three-dimensional spirals of atomic layered MoS<sub>2</sub>.

### Permalink

<https://escholarship.org/uc/item/0dj9w5rk>

### Journal

Nano letters, 14(11)

### ISSN

1530-6984

### Authors

Zhang, Liming

Liu, Kaihui

Wong, Andrew Barnabas

et al.

### Publication Date

2014-11-01

### DOI

10.1021/nl502961e

Peer reviewed

# Three-dimensional Spirals of Atomic Layered MoS<sub>2</sub>

Liming Zhang\*<sup>1</sup>, Kaihui Liu\*<sup>2,3</sup>, Andrew Barnabas Wong<sup>1</sup>, Jonghwan Kim<sup>2</sup>, Xiaoping  
Hong<sup>2</sup>, Chong Liu<sup>1,4</sup>, Ting Cao<sup>2</sup>, Steven G Louie<sup>2,4</sup>, Feng Wang<sup>2,4,5</sup>  
and Peidong Yang<sup>1,4,5,6</sup>

<sup>1</sup>Department of Chemistry, University of California at Berkeley, Berkeley, CA 94720,  
United States

<sup>2</sup>Department of Physics, University of California at Berkeley, Berkeley, CA 94720,  
United States

<sup>3</sup>State Key Laboratory for Mesoscopic Physics and Collaborative Innovation Centre  
of Quantum Matter, Peking University, Beijing 100871, China

<sup>4</sup>Materials Science Division, Lawrence Berkeley National Laboratory, Berkeley,  
California 94720, United States

<sup>5</sup>Kavli Energy NanoSciences Institute at the University of California, Berkeley and  
the Lawrence Berkeley National Laboratory, Berkeley, CA 94720, United States

<sup>6</sup>Department of Material Science and Engineering, University of California at  
Berkeley, Berkeley, CA 94720, United States

\*These two authors contribute equally to this work

Atomically thin two-dimensional (2D) layered materials, including graphene, boron nitride and transition metal dichalcogenides (TMDs), can exhibit novel phenomena distinct from their bulk counterparts<sup>1-4</sup> and hold great promise for novel electronic and optoelectronic applications<sup>5-10</sup>. Controlled growth of such 2D materials with different thickness, composition, and symmetry are of central importance to realize their potential. In particular, the ability to control the symmetry of TMD layers is highly desirable because breaking the inversion symmetry can lead to intriguing valley physics<sup>11-13</sup>, nonlinear optical properties<sup>14</sup>, and piezoelectric responses<sup>15</sup>. Here we report the first growth of spirals of layered MoS<sub>2</sub> with atomically thin helical periodicity, which exhibits a chiral structure and breaks the three-dimensional (3D) inversion symmetry explicitly. The spirals composed of tens of connected MoS<sub>2</sub> layers with decreasing areas: each basal plane has a triangular shape and shrinks gradually to the summit when spiraling up. All the layers in the spiral assume an AA lattice stacking, in contrast to the centrosymmetric AB stacking in natural MoS<sub>2</sub> crystals. We show that the non-centrosymmetric MoS<sub>2</sub> spiral leads to a strong bulk second-order optical nonlinearity. In addition, we found that the growth of spirals involves a dislocation mechanism, which can be generally applicable to other 2D TMD materials.

Transition metal dichalcogenides (TMDs), a family of atomically thin 2D materials, have attracted much research interest due to their novel layer-dependent electronic and optical properties. For instance, monolayer MoS<sub>2</sub> exhibits a direct optical bandgap of ~1.8 eV in the visible range<sup>3, 4</sup>, a large exciton binding energy of ~1 eV<sup>10</sup>, an emerging valley degree of freedom<sup>11-13</sup>, and a strong second-order optical nonlinearity<sup>14</sup>, which are promising for novel applications ranging from nano-electronics<sup>7</sup> and photonics<sup>8</sup> to photovoltaics<sup>9</sup> and valleytronics<sup>11-13</sup>. Many of the intriguing properties of monolayer MoS<sub>2</sub>, such as valley polarizations and the second order nonlinearity, originate from its non-centrosymmetric structure compared with centrosymmetric bilayers or bulk MoS<sub>2</sub>. Many other physical properties, such as piezoelectric responses and Pockels effects, also emerge only when the inversion symmetry is broken<sup>15</sup>. To better explore the effect of symmetry in layered TMDs, it is highly desirable to synthesize TMD structures with controlled symmetry properties. The spiral is an intriguing structure that can be found in nature and artificial materials. Spiral structures are chiral and automatically break the reflection and inversion symmetry. Previously nanoscale spirals have been realized in nanoplates<sup>16</sup>, nanotubes<sup>17</sup> and Eshelby twisted nanowires<sup>18, 19</sup>. Here we show that spirals of atomic layered MoS<sub>2</sub> involving screw dislocations can also be grown directly using chemical vapor deposition (CVD), and these MoS<sub>2</sub> spirals exhibit interesting physical properties.

Large-sized highly crystalline MoS<sub>2</sub> monolayer was successfully grown by CVD method recently<sup>20-22</sup>. To grow the atomic layered spiral structures, we developed an

approach based on these previous methods but with modified growth conditions (See Methods and Supplementary information S1). Our key control is to increase the nucleation rate at the initial stage to generate a dislocation center with high spiraling-up activity. We can grow spiral structures on various substrates, including SiO<sub>2</sub>/Si, mica, fused silica, and TiO<sub>2</sub> with yield as high as 80% (the other 20% are mainly monolayers).

The morphology of our spiral structures was characterized by atomic force microscopy (AFM). Fig. 1a shows an illustration of the 3D spiral structure, and Figs 1b-e show the AFM images of several spirals grown on fused silica with size around 300 nm (defined by the edge length of the largest basal plane). The height images (Fig. 1b,c) show obvious plateaus with step height of about 0.62 nm, which matches the thickness of single MoS<sub>2</sub> atomic layer<sup>23</sup>. The layer thickness of 0.62 nm could also be independently determined by the X-ray diffraction (XRD) technique (Supplementary information S2). The spirals can be either left or right-handed (Fig. 1d) with equal probability. When the spiral density is high, twin- or mirror twin-like spiral structures can be found (Fig. 1e). The size of the spirals can be tuned in the range of about 100 nm to 20 μm by the growing conditions. Shown in Fig. 1f is a typical bright-field optical image of large-sized spirals (~10 μm). They overall look like pyramids: each basal plane has a triangular shape and shrinks gradually to the summit point. The AFM images of large spirals (Supplementary information S3) show that these “pyramids” have tens of spiral layers.

To confirm the atomic layered spirals originate from MoS<sub>2</sub> layers, we first carried

out reflection spectroscopic measurements on fused silica. The reflection spectrum (Fig. 1g) shows two prominent peaks at 1.80 eV and 1.95 eV, in accordance with the two fingerprint exciton transitions in MoS<sub>2</sub><sup>3</sup>. X-ray photoelectron spectroscopy (XPS) was also used to study the elemental composition of spirals (Supplementary information S4). It shows four obvious peaks at 229.0, 232.1, 162.2 and 163.4 eV, which can be attributed to the doublet of Mo 3d<sub>5/2</sub> and 3d<sub>3/2</sub>, S 2p<sub>3/2</sub> and 2p<sub>1/2</sub> in MoS<sub>2</sub>, respectively<sup>24</sup>.

In order to gain microscopic structure information of the MoS<sub>2</sub> spirals, we employed transmission electron microscopy (TEM) to study the crystal structure of spirals transferred onto TEM grids (See Methods for transfer procedure). Fig. 2a shows one typical TEM image of a 300 nm sized MoS<sub>2</sub> spiral. Clear spiral features as in the AFM images can be identified: the triangles spiral up layer by layer to the center summit. Microscopically, a monolayer MoS<sub>2</sub> consists of two triangle lattices of S atoms and a sheet of Mo atoms occupying trigonal prismatic sites between the S sheets<sup>25</sup>, which forms a hexagonal structure with Mo and S atoms when projected onto the 2D basal plane (Fig. 2b). However, high-resolution TEM (HRTEM) images and diffraction patterns of monolayer MoS<sub>2</sub> typically show trigonal lattice structures<sup>20-22</sup>. Our spiral structures here exhibit similar features as that in monolayer MoS<sub>2</sub>. The HRTEM image (Fig. 2c) taken at the center of the spiral in Fig. 2a shows a trigonal lattice with the distance of adjacent bright spots equal to the in-plane Mo-Mo distance of 3.15 Å. The selected area electron diffraction (SAED) taken from the same region shows a single set of pattern characteristic of trigonal structures (Fig. 2d),

indicating that different spiral layers are of the same crystal orientation. However, the intensity ratio between the  $[-2\ 1\ 1\ 0]$  and  $[1\ -1\ 0\ 0]$  diffraction points is about 2.5, which is quite different from 1.1 as observed in monolayers<sup>21</sup>. It suggests that the adjacent spiral layers have a displacement similar to that in Bernal stacked bilayer graphene<sup>26</sup>.

Two possible MoS<sub>2</sub> stacking orders are compatible with the lattice pattern observed in the HRTEM (Fig. 2c) and electron diffraction (Fig. 2d). These two stacking orders, referred to as AB and AA stacking, are illustrated in the inset of Fig. 3a. For AB stacking, the in-plane Mo-S bond directions are opposite for the two adjacent layers and the crystal structure belongs to the centrosymmetric  $D_{3d}^1$  group. The AA stacked MoS<sub>2</sub>, however, have the in-plane Mo-S bonds pointing to the same direction in adjacent layers, and it belongs to the non-centrosymmetric  $D_{3h}^1$  group. Theoretical calculations based on local-density approximation (LDA) show that the AA and AB stacked MoS<sub>2</sub> are both stable configurations with very similar total energy (For AA stacking order, the staggered stacking configuration is energetically more favorable than the eclipsed configuration. See Supplementary information S5 for details). Natural MoS<sub>2</sub> crystals usually assume the AB-stacked centrosymmetric configuration. For our CVD-grown MoS<sub>2</sub> spirals, all layers show triangular shapes with parallel edges (Fig. 1b,d and Fig. 2a). Because MoS<sub>2</sub> layers are known to have Mo-terminated zigzag edges<sup>27</sup>, the same triangular orientation in different layers indicates that our MoS<sub>2</sub> spirals are composed of helical layers with AA stacking order. Such AA stacking explicitly breaks the inversion symmetry that presents in bulk

MoS<sub>2</sub> crystals, and it can lead to dramatic changes in symmetry-dependent properties of MoS<sub>2</sub> ranging from optical nonlinearity and electro-optics to piezoelectric and valley physics.

Here we examine the second-order optical nonlinearity in the MoS<sub>2</sub> spirals using optical second-harmonic generation (SHG). The SHG signal is extremely sensitive to the symmetry, and it vanishes for any material with inversion symmetry (within the dipole approximation)<sup>14</sup>. For MoS<sub>2</sub>, it has been demonstrated that the non-centrosymmetric monolayer exhibits strong SHG signals (black curve in Fig. 3a), but the centrosymmetric AB stacked bilayer has no SHG due to destructive interference between the signals from the two layers. In fact, the SHG signal from a thick AB-stacked MoS<sub>2</sub> crystal is much weaker than that of a monolayer due to the centrosymmetric AB stacking (red curve in Fig. 3a)<sup>14</sup>. For AA stacked MoS<sub>2</sub>, which breaks the inversion center, the SHG signal can increase dramatically with the layer thickness because the signals from different layers interfere constructively with each other. Approximately, SHG should scale as  $N^2$  for MoS<sub>2</sub> thin layers, where  $N$  is the MoS<sub>2</sub> layer number<sup>28</sup>. Indeed our spiral structures show very strong SHG (blue curve in Fig. 3a). For 6  $\mu\text{m}$ -sized spirals (with a layer number  $\sim 15$ ), the SHG signal is almost two orders of magnitude higher than that of a MoS<sub>2</sub> monolayer, in striking contrast to AB-stacked multilayers (red curve in Fig. 3a). This remarkably strong SHG in MoS<sub>2</sub> spirals confirms unambiguously that the different layers are indeed AA stacked with broken inversion symmetry.

Next we examine the vibrational properties of the AA-stacked MoS<sub>2</sub> spirals using



Raman spectroscopy. The Raman spectra in the range of 350~470  $\text{cm}^{-1}$  from MoS<sub>2</sub> monolayers, AB-stacked multilayers, and the AA-stacked spirals were compared in Fig. 3b. The two prominent Raman peaks around 383 and 407  $\text{cm}^{-1}$  correspond to the *in-plane* E<sub>2g</sub><sup>1</sup> and *out-of-plane* A<sub>1g</sub> vibrational modes, respectively. It has been established that the interlayer van der Waals coupling in AB stacked multilayer can soften the E<sub>2g</sub><sup>1</sup> mode and stiffen the A<sub>1g</sub> mode compared with that in a monolayer<sup>29</sup>. The same trend is observed in AA-stacked MoS<sub>2</sub> spirals, which indicates that the layers in a spiral have comparable mechanical coupling as those in AB-stacked multilayers.

We further explored the photoluminescence (PL) properties of the MoS<sub>2</sub>spirals. Fig. 3c shows typical PL spectra from MoS<sub>2</sub> monolayers, AB stacked multilayers, and spirals. The relatively sharp peak I around 670 nm originates from the lowest-energy exciton transition of MoS<sub>2</sub>. Monolayer MoS<sub>2</sub> is a direct bandgap material and therefore has very strong PL emission. AB-stacked multilayer MoS<sub>2</sub>, on the other hand, has an indirect bandgap. This leads to a strongly reduced PL at peak I (about 1/30 of that in a monolayer), and creates a new PL peak II at 950 nm due to the indirect exciton transition. (The small red-shift of peak I can be attributed to the interlayer coupling<sup>3, 4</sup>). For spiral structures, the PL of peak I is as weak as that in AB stacked multilayer. Our theoretical calculations show that AA-stacked MoS<sub>2</sub> layers also have an indirect bandgap (Supplementary information S6). However, it is quite unusual that peak II nearly disappears. We tentatively attribute this behavior to the non-radiative recombination of excitons (electron-hole pair) at the extensive metallic

edges present in the spiral samples<sup>29</sup>.

Finally, we investigate the growth mechanism for atomic-layered MoS<sub>2</sub> spirals. According to *Burton-Cabrera-Frank* (BCF) theory<sup>30</sup>, screw dislocations can lead to the growth of spiral structures<sup>16-19</sup>. The screw dislocation is highly strained and locates at the centre of the spiral structures. The formation of a screw dislocation core in MoS<sub>2</sub> spirals requires the generation of slipped planes (screw defects) in the bottom layer (shown in Fig. 4a), otherwise the growth will follow an *in-plane-growth* mode and produce monolayers of MoS<sub>2</sub><sup>20-22</sup>. In our refined CVD growth conditions, the seeding of the screw defects was achieved by introducing a spike of sulfur supersaturation at the initial stage of the reaction. The higher partial pressure of sulfur greatly increases the possibility of accidental overgrowth of two exposed edges, which can lead to a slipped edge with a screw defect (Fig. 4a). Once a screw dislocation is created, it will remain active and gradually grow in the vertical direction because continued growth at the edge sites of the dislocation center is energetically favorable. The exposing edges continue to grow with the preference to form a triangular corner on each step monolayer (turning 120 degree each time and exposing the low energy Mo-Mo zigzag edge out<sup>27</sup>). Since the upper layer is formed later and has shorter time to grow, the pyramid-shaped 3D atomic layered MoS<sub>2</sub> spiral will be created (Figs 4b-d). Some clues of this growth mechanism can be found from the AFM images taken at different growth stages (Fig. 4e-h). Similar to our schematic model, the spiral will grow from a slipped edge (Fig. 4e) and generate a small spiraled triangle (Fig. 4f). The generated dislocation core will keep spiraling up and form a

pyramid-shaped 3D large spiral finally (Fig. 4g, h). We note that the bottom layer is not perfectly triangular, likely due to fast non-equilibrium growth conditions at the initial stage. Newly generated layers from a dislocation can grow on top of the bottom layer. On top of these spirals, the dislocation core can be clearly identified.

The MoS<sub>2</sub> spirals are the product of both screw-dislocation driven growth of the core along the vertical dimension and triangular layer expansion along the lateral dimension. The elementary Burgers vector of the screw dislocations in the layered MoS<sub>2</sub> is just one unit cell. Since the upper layers are formed later and have shorter time to grow, the lateral layer size decreases with the height and the spiral forms an overall pyramid-like shape. The pyramid slope is determined by the growth velocity ratio between the vertical dislocation growth and lateral monolayer expansion. Because a large strain is present at the dislocation core, the vertical growth is significantly slower than the lateral expansion. Typically we found the in-plane monolayer growth rate is 50~100 times faster than the vertical nucleation centre for 300 nm spirals and 300~500 times for 20 μm spirals. The larger ratio in bigger spirals is presumably due to the decreased supersaturation over time in our growth condition (Supplementary information S1). We believe that this mechanism of spiral growth is not limited to MoS<sub>2</sub>. Many other 2D atomic layered materials with strong *in-plane* covalent bonding and weak *out-of-plane* van der Waals interaction, such as WS<sub>2</sub>, MoSe<sub>2</sub> and WSe<sub>2</sub>, share similar CVD growth mechanism<sup>25</sup>. Therefore systematical optimizing the growth conditions will create a family of spiraled 2D layers of TMDs.

In summary, we grow and characterize spiral structure of atomic layered MoS<sub>2</sub>

for the first time. These non-centrosymmetric TMD spirals, in contrary to their centrosymmetric bulk crystals, can lead to new behavior in electro-optic, piezoelectric, and nonlinear optical responses as well as valley physics, which may find applications in nanoscale electronic and optical devices.

## **Methods:**

### **Growth of atomic layered MoS<sub>2</sub> spirals**

We grew MoS<sub>2</sub> spirals by CVD on various substrates using MoO<sub>3</sub> and S powder as precursors. The substrate was loaded into the 1-inch CVD furnace and placed face-down above one crucible containing 5.0~7.5 mg of MoO<sub>3</sub> ( $\geq 99.5\%$ , sigma-Aldrich) with another crucible containing 140 mg of S ( $\geq 99.5\%$ , sigma-Aldrich). The key difference between the growth of spirals and monolayer MoS<sub>2</sub> is the location temperature regions of S. In order to increase the possibility to get spirals, S was loaded in the high temperature region close to MoO<sub>3</sub>. The CVD process was performed under ambient pressure while flowing ultrahigh-purity nitrogen. The recipe is: sit 1 h at 105 °C with 500 sccm, ramp to 700 °C at 15 °C/min with 10~15 sccm N<sub>2</sub>, sit 5 min at 700 °C and cool down naturally with 500 sccm gas flow. The domain size of MoS<sub>2</sub> spirals could be tuned from several hundreds of nanometers to tens of micrometers depending on growth conditions. More detailed information on the growth of spirals and monolayer MoS<sub>2</sub> can be found in the Supplementary information S1.

## Sample Characterization

- (1) Atomic force microscope (Veeco Nanoscope) in tapping mode was used for morphology studies of MoS<sub>2</sub> spirals.
- (2) TEM images and electron diffraction patterns were taken by JEOL 2100 at an accelerating voltage of 200 kV. TEM samples were transferred from the as-grown substrate and procedure is shown below. Polymer transfer layers were prepared by spin-coating poly(methyl methacrylate)(PMMA) A4 onto fused silica chips (MoS<sub>2</sub> side) at 3000 r.p.m. for 60 s to form ~200 nm thick layer. The chips were floated on HF aqueous solution (10 wt%) for several hours. The HF etched fused silica slowly, causing the chips to fall off and leaving the MoS<sub>2</sub> coated PMMA film floating on the solution surface. The membrane was transferred to deionized water two times, and then scooped onto TEM grid and dried. The PMMA film was removed by baking the TEM grid at 350 °C in N<sub>2</sub>/H<sub>2</sub> gas (500/20 sccm) flow for 2 h at atmospheric pressure.
- (3) Reflection spectra were taken by our home-built system. A supercontinuum laser (470 nm ~ 1800 nm) is used as the light source. We focus the supercontinuum down to ~2 μm, and analyze the signal with a spectrograph equipped with an array charged coupled device (CCD) detector. Two sets of reflection spectra with the MoS<sub>2</sub> spiral inside beam ( $I_{\text{inside}}$ ) and outside beam ( $I_{\text{outside}}$ ) are taken and the final spectrum is obtained as  $\Delta R/R = (I_{\text{inside}} - I_{\text{outside}})/I_{\text{outside}}$ .
- (4) SHG signal were taken by our home built setup. We use femtosecond pulses with

1.8  $\mu\text{m}$  wavelength and 250 fs pulse width, which is generated by an optical parametric amplifier (OPA). OPA is pumped by femtosecond pulses at 1026 nm (at a repetition rate of 100 kHz) from a regenerative amplifier seeded by a mode-locked oscillator (Light Conversion PHAROS). SHG signal with 900 nm wavelength was collected in the back scattering geometry via confocal microscope and analyzed by a monochromator equipped with liquid nitrogen cooled CCD. Beam size of fundamental light is  $\sim 2\mu\text{m}$  and fluence is  $\sim 25\text{ mJ}/\text{cm}^2$ .

(5) Raman spectroscopy and photoluminescence were taken by a Horiba HR800 system with laser excitation energy of 532 nm. The laser spot size is  $\sim 1\mu\text{m}$  and a laser power of  $\sim 5\text{ mW}$  was used to avoid heating and PL saturation.

(6) XPS measurements were carried out using a Kratos Axis Ultra spectrometer with Al  $\text{K}\alpha$  monochromated X-ray at low pressures of  $5\times 10^{-9}$  to  $1\times 10^{-8}$  Torr. The collection area was about  $300\times 700\mu\text{m}^2$ . The highest peak in C1s spectra was shift to 284.8 eV for charge correction.

**Acknowledgement:** This work was supported by the Director, Office of Science, Office of Basic Energy Sciences, Materials Sciences and Engineering Division, of the U.S. Department of Energy under Contract No. DE-AC02-05CH11231(P-Chem) and No. DE-SC0003949 (Early Career Award). We thank the Molecular Foundry and Lawrence Berkeley National Laboratory for use of their facilities. We would especially like to thank Prof. William Nix at Stanford University for the help

discussion on the formation mechanism of spirals. Dr. K. Liu acknowledges support from National Program for Thousand Young Talents of China.

## Figure captions:

**Figure 1 | Morphology of atomic layered MoS<sub>2</sub> spirals.** **a**, Schematic illustration of the MoS<sub>2</sub> spiral. **b-c**, AFM image (height signal) of 300 nm large (defined as the length of bottom triangle) spiral. The profile (c) is taken along the dotted line in (b), showing obvious plateaus (marked by  $\alpha$ ,  $\beta$ ,  $\gamma$  and  $\delta$ ) with step height of about 0.62 nm. **d**, AFM image (phase signal) of MoS<sub>2</sub> spirals with left (upper) and right (lower) handedness. **e**, AFM image (phase signal) of MoS<sub>2</sub> spiral with two screws inside, exhibiting twin like structure. **f**, Bright-field optical image of ~10  $\mu\text{m}$ -sized spirals. They overall look like pyramids: each basal plane has a triangular shape and shrinks gradually to the summit point. **g**, Reflection spectrum of spiral on fused silica substrate.

**Figure 2 | Crystal structure of atomic layered MoS<sub>2</sub> spiral.** **a**, Representative TEM image from one MoS<sub>2</sub> spiral. It shows clear spiral features: the triangles spiral up layer by layer to the centre summit. **b**, Top view of monolayer 2D hexagonal lattice structure and side view of a unit cell of the MoS<sub>2</sub> lattice structure. **c-d**, High-resolution TEM (HRTEM) image (c) and selected area electron diffraction (SAED) pattern (d) obtained in the center of the MoS<sub>2</sub> spiral in (a). The same trigonal symmetry as in monolayer indicates that the spiral layers are of same lattice structure. **e**, Intensity profiles taken along the dashed white box in (d). The intensity profile is different from that in monolayer indicates that the spiral layers have a well-defined stacking order.



**Figure 3 | Stacking and interlayer coupling in atomic layered MoS<sub>2</sub> spiral.** **a**, Nonlinear optical second-harmonic generation (SHG) signal from monolayer, AB stacked multilayer and our AA stacked spiral of MoS<sub>2</sub>. Insets show the side view of AA and AB stacked multilayer lattice, respectively. **b**, The Raman spectra in the range of 350~470 cm<sup>-1</sup> from monolayer, AB stacked multilayer and spiral, showing the E<sub>2g</sub><sup>1</sup> and A<sub>1g</sub> modes. The spectra are displaced along the vertical axis for clarity. **c**, Photoluminescence (PL) spectra for monolayer, AB stacked multilayer and spiral. The PL spectra have been displaced along the vertical axis for clarity.

**Figure 4 | Growing mechanism of atomic layered MoS<sub>2</sub> spiral.** **a-d**, Schematic illustration of MoS<sub>2</sub> spiral from nucleation to growth. Black lines indicate the exposed edges. **e-h**, AFM images (phase signal) of several typical spirals at different growth stages. The growth will start from a slipped edge (e) and generate a small spiraled triangle(f). With growth continued, the generated dislocation core will keep spiraling up vertically and form pyramid-shaped 3D large spirals (g, h).

## References:

1. Novoselov, K.S. et al. Two-dimensional gas of massless Dirac fermions in graphene. *Nature***438**, 197-200 (2005).
2. Zhang, Y.B., Tan, Y.W., Stormer, H.L. & Kim, P. Experimental observation of the quantum Hall effect and Berry's phase in graphene. *Nature***438**, 201-204 (2005).
3. Mak, K.F., Lee, C., Hone, J., Shan, J. & Heinz, T.F. Atomically Thin MoS<sub>2</sub>: A New Direct-Gap Semiconductor. *Phys. Rev. Lett.***105**, 136805 (2010).
4. Splendiani, A. et al. Emerging photoluminescence in monolayer MoS<sub>2</sub>. *Nano Lett.***10**, 1271-1275 (2010).
5. Bonaccorso, F., Sun, Z., Hasan, T. & Ferrari, A.C. Graphene photonics and optoelectronics. *Nat. Photonics***4**, 611-622 (2010).
6. Dean, C. et al. Boron nitride substrates for high-quality graphene electronics. *Nat.Nanotechnol.* **5**, 722-726 (2010).
7. Radisavljevic, B., Radenovic, A., Brivio, J., Giacometti, V. & Kis, A. Single-layer MoS<sub>2</sub> transistors. *Nat.Nanotechnol.* **6**, 147-150 (2011).
8. Lopez-Sanchez, O., Lembke, D., Kayci, M., Radenovic, A. & Kis, A. Ultrasensitive photodetectors based on monolayer MoS<sub>2</sub>. *Nat.Nanotechnol.* **8**, 497-501 (2013).
9. Feng, J., Qian, X.F., Huang, C.W. & Li, J. Strain-engineered artificial atom as a broad-spectrum solar energy funnel. *Nat. Photonics***6**, 865-871 (2012).
10. Qiu, D.Y., Felipe, H. & Louie, S.G. Optical Spectrum of MoS<sub>2</sub>: Many-Body Effects and Diversity of Exciton States. *Phys. Rev. Lett.***111**, 216805 (2013).
11. Mak, K.F., He, K.L., Shan, J. & Heinz, T.F. Control of valley polarization in monolayer MoS<sub>2</sub> by optical helicity. *Nat.Nanotechnol.* **7**, 494-498 (2012).
12. Zeng, H.L., Dai, J.F., Yao, W., Xiao, D. & Cui, X.D. Valley polarization in MoS<sub>2</sub> monolayers by optical pumping. *Nat.Nanotechnol.* **7**, 490-493 (2012).
13. Cao, T. et al. Valley-selective circular dichroism of monolayer molybdenum disulphide. *Nat.Comm.* **3**, 887 (2012).
14. Li, Y. et al. Probing symmetry properties of few-layer MoS<sub>2</sub> and h-BN by optical second-harmonic generation. *Nano Lett.***3**, 3329-3333 (2013).
15. Duerloo, K.-A.N., Ong, M.T. & Reed, E.J. Intrinsic piezoelectricity in two-dimensional materials. *J. Phys. Chem. Lett.* **3**, 2871-2876 (2012).
16. Morin, S.A., Forticaux, A., Bierman, M.J. & Jin, S. Screw dislocation-driven growth of two-dimensional nanoplates. *Nano Lett.* **11**, 4449-4455 (2011).
17. Morin, S.A., Bierman, M.J., Tong, J. & Jin, S. Mechanism and kinetics of spontaneous nanotube growth driven by screw dislocations. *Science***328**, 476-480 (2010).
18. Bierman, M.J., Lau, Y.K.A., Kvit, A.V., Schmitt, A.L. & Jin, S. Dislocation-driven nanowire growth and Eshelby twist. *Science***320**, 1060-1063 (2008).
19. Zhu, J. et al. Formation of chiral branched nanowires by the Eshelby Twist. *Nat.Nanotechnol.* **3**, 477-481 (2008).
20. Lee, Y.H. et al. Synthesis of Large-Area MoS<sub>2</sub> Atomic Layers with Chemical Vapor Deposition. *Adv. Mater.* **24**, 2320-2325 (2012).
21. van der Zande, A.M. et al. Grains and grain boundaries in highly crystalline monolayer molybdenum disulphide. *Nat. Mater.* **12**, 554-561 (2013).

22. Najmaei, S. et al. Vapour phase growth and grain boundary structure of molybdenum disulphide atomic layers. *Nat. Mater.* **12**, 754-759 (2013).
23. Winer, W.O. Molybdenum disulfide as a lubricant - A review of fundamental knowledge. *Wear***10**, 422-452 (1967).
24. Wang, H.W., Skeldon, P. & Thompson, G.E. XPS studies of MoS<sub>2</sub> formation from ammonium tetrathiomolybdate solutions. *Surf. Coat. Technol.***91**, 200-207 (1997).
25. Chhowalla, M. et al. The chemistry of two-dimensional layered transition metal dichalcogenide nanosheets. *Nature Chem.* **5**, 263-275 (2013).
26. Meyer, J.C. et al. The structure of suspended graphene sheets. *Nature***446**, 60-63 (2007).
27. Lauritsen, J.V. et al. Size-dependent structure of MoS<sub>2</sub> nanocrystals. *Nat. Nanotechnol.* **2**, 53-58 (2007).
28. Shen Y. R. *The Principles of Nonlinear Optics*. (J. Wiley & Sons Inc. press, Hoboken, New Jersey, 2003).
29. Lee, C. et al. Anomalous Lattice Vibrations of Single- and Few-Layer MoS<sub>2</sub>. *ACS Nano***4**, 2695-2700 (2010).
30. Burton, W.K., Cabrera, N. & Frank, F.C. The growth of crystals and the equilibrium structure of their surfaces. *Philosophical Transactions of the Royal Society of London Series a-Mathematical and Physical Sciences***243**, 299-358 (1951).

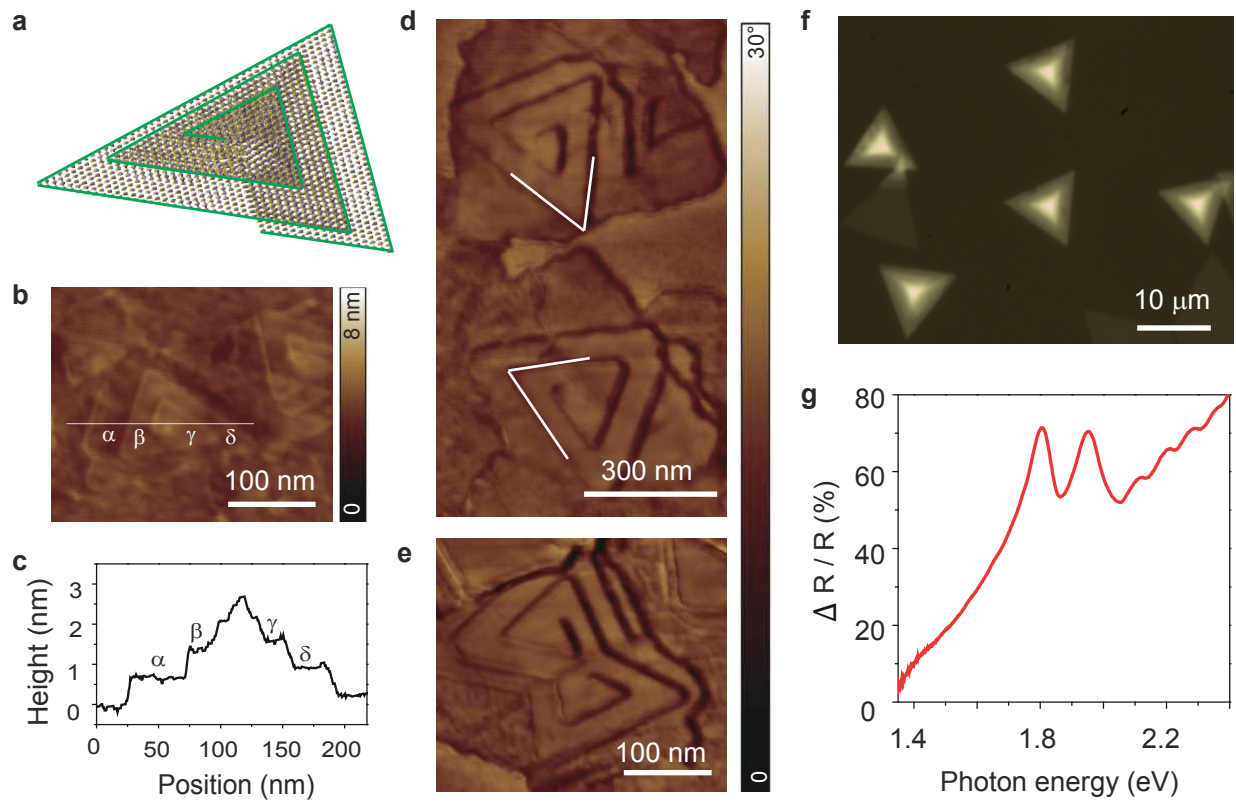


Figure 1

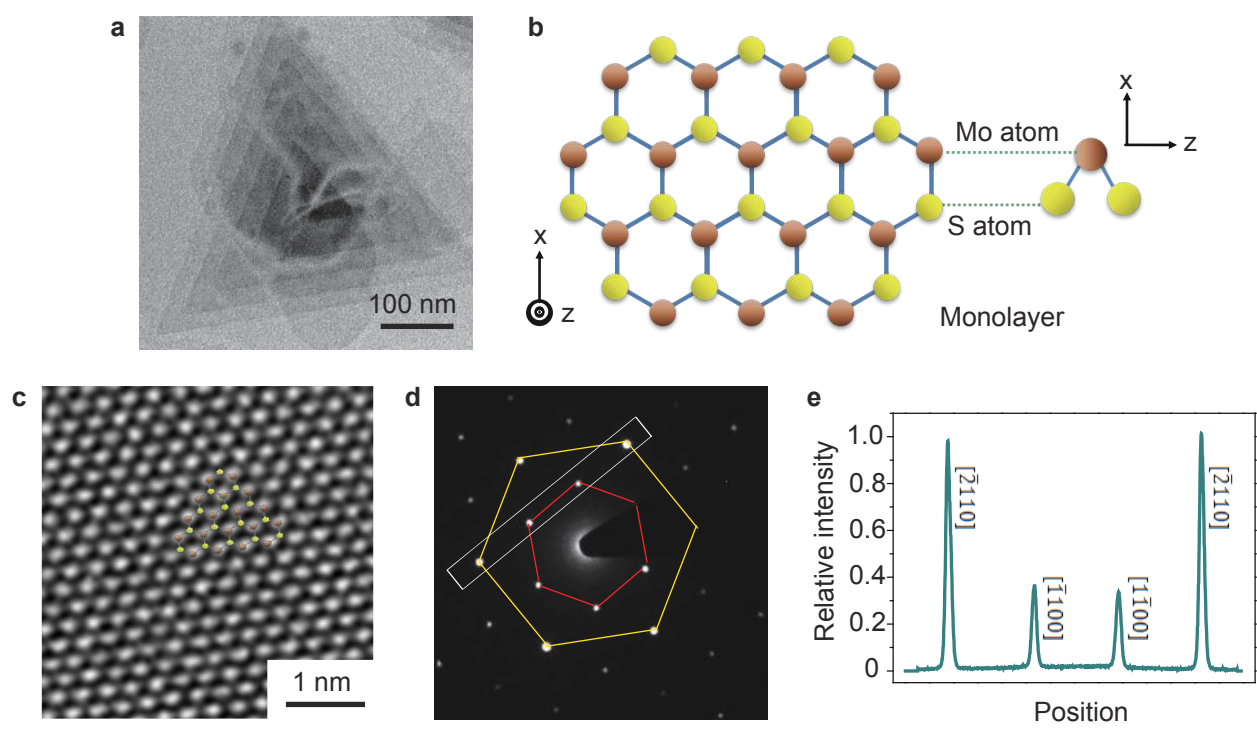
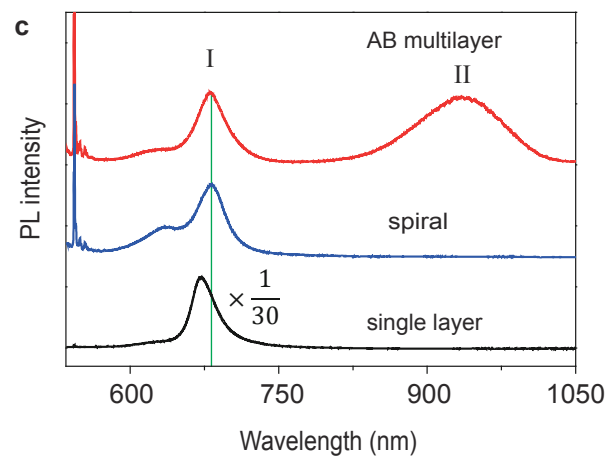
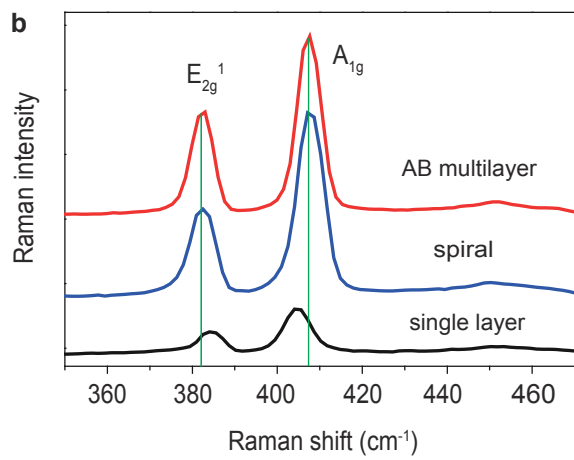
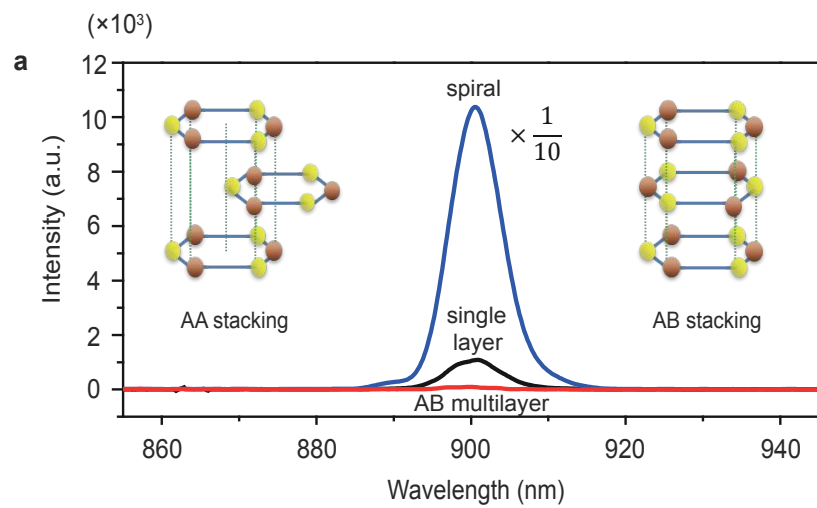


Figure 2



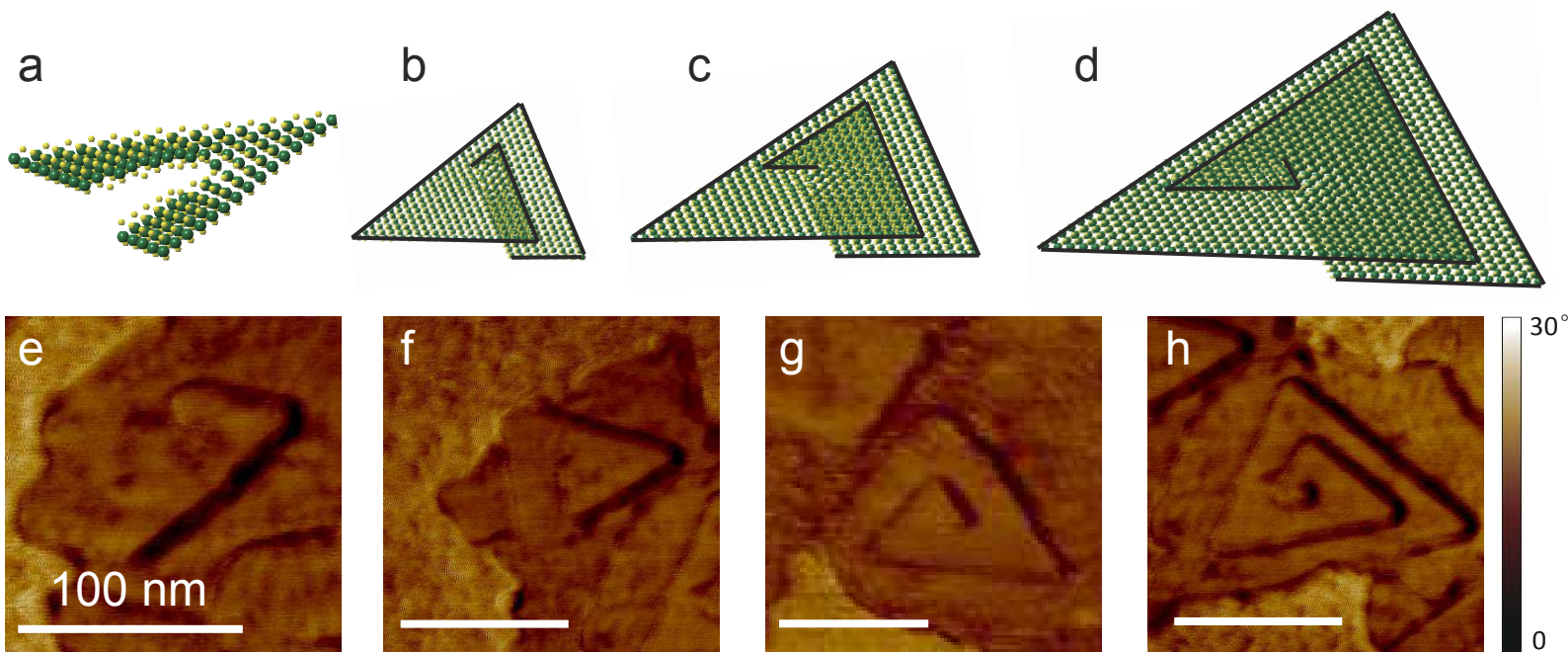


Figure 4